atmosphere

MDPI

Review

Moist Orographic Convection: Physical Mechanisms and Links to Surface-Exchange Processes

Daniel J. Kirshbaum [1,*], Bianca Adler [2], Norbert Kalthoff [2], Christian Barthlott [3] and Stefano Serafin [4]

1 Department of Atmospheric and Oceanic Sciences, McGill University, Montréal, QC H3A 0B9, Canada
2 Institute of Meteorology and Climate Research, Karlsruhe Institute of Technology (KIT), D-76344 Eggenstein-Leopoldshafen, Germany; bianca.adler@kit.edu (B.A.); norbert.kalthoff@kit.edu (N.K.)
3 Institute of Meteorology and Climate Research, Karlsruhe Institute of Technology (KIT), D-76131 Karlsruhe, Germany; christian.barthlott@kit.edu
4 University of Vienna, Department of Meteorology and Geophysics, 1090 Vienna, Austria; stefano.serafin@univie.ac.at
* Correspondence: daniel.kirshbaum@mcgill.ca; Tel.: +1-514-398-3347

Received: 11 January 2018; Accepted: 21 February 2018; Published: 25 February 2018

Abstract: This paper reviews the current understanding of moist orographic convection and its regulation by surface-exchange processes. Such convection tends to develop when and where moist instability coincides with sufficient terrain-induced ascent to locally overcome convective inhibition. The terrain-induced ascent can be owing to mechanical (airflow over or around an obstacle) and/or thermal (differential heating over sloping terrain) forcing. For the former, the location of convective initiation depends on the dynamical flow regime. In "unblocked" flows that ascend the barrier, the convection tends to initiate over the windward slopes, while in "blocked" flows that detour around the barrier, the convection tends to initiate upstream and/or downstream of the high terrain where impinging flows split and rejoin, respectively. Processes that destabilize the upstream flow for mechanically forced moist convection include large-scale moistening and ascent, positive surface sensible and latent heat fluxes, and differential advection in baroclinic zones. For thermally forced flows, convective initiation is driven by thermally direct circulations with sharp updrafts over or downwind of the mountain crest (daytime) or foot (nighttime). Along with the larger-scale background flow, local evapotranspiration and transport of moisture, as well as thermodynamic heterogeneities over the complex terrain, regulate moist instability in such events. Longstanding limitations in the quantitative understanding of related processes, including both convective preconditioning and initiation, must be overcome to improve the prediction of this convection, and its collective effects, in weather and climate models.

Keywords: moist convection; orography; mesoscale; cumulus clouds; precipitation

1. Introduction

Orographic ascent enhances precipitation by lifting air to saturation, increasing the hydrometeor content of impinging clouds, and initiating moist instabilities. This precipitation feeds vegetation, rivers, and streams, and provides critical freshwater storage in snowpack and glaciers. However, orography may also suppress precipitation by forcing descent, blocking moist impinging flow, inducing vertical mixing with dry air aloft, and depleting atmospheric moisture. As a result, mountain ranges often exhibit dramatic mesoscale gradients in annual precipitation (e.g., [1–4]). Given the profound importance of orographic precipitation for regional ecosystems and for generating hazardous weather (thunderstorms, hail, flash floods, etc.), its conceptual understanding and accurate prediction are essential.

Orographic precipitation can be broadly separated into two categories: stratiform and convective. Whereas the former is produced by nominally statically stable clouds with positive squared moist Brunt-Väisälä frequency ($N_m^2 > 0$), the latter is produced by cumuliform, statically unstable clouds with $N_m^2 < 0$. The sign of N_m^2 depends on the vertical profile of the equivalent potential temperature (θ_e), total water mixing ratio (q_t), temperature, and pressure [5,6]. Because the latter two variables are not conserved following the flow, the potential for orographic convection cannot be unambiguously deduced from an upstream sounding profile.

The terrain-forced lifting required for orographic precipitation is caused by a range of different physical mechanisms. Arguably the most well-known of these mechanisms are mechanical in nature, involving forced ascent of impinging flow over sloping surfaces and dynamically forced horizontal convergence upstream and/or downstream of a barrier [7]. In statically stable flows, vertically propagating mountain waves can extend these motions deep into the troposphere, giving rise to deep precipitating cloud layers. In the presence of a precipitating, non-orographic "seeder" cloud, even modest forced lifting can greatly enhance precipitation. This enhancement is owing to the large water supply and precipitation efficiency of the low-level orographic "feeder" cloud (e.g., [8,9]).

Orographic lifting may also stem from local baroclinicity induced by daytime insolation or nocturnal radiative cooling over complex terrain. Such thermal forcing drives thermally direct vertical circulations, with flow generally directed up (down) the mountain during the day (night). Because the ascending branches of such circulations are mostly confined to the atmospheric boundary layer (ABL) (e.g., [10]), they generally do not saturate the flow over a deep enough layer to produce stratiform precipitation. Thus, this mechanism is primarily associated with convective precipitation.

The majority of past research on orographic precipitation has focused on the stratiform, mechanically forced type, which is a challenging problem in its own right. Less attention has been devoted to the more complex problem of convective precipitation, despite its importance to many tropical, subtropical, and midlatitude regions. This review article seeks to condense the modern understanding of this subject and identify related unresolved questions in need of further investigation. Another objective is to characterize the link between orographic convection and surface exchange processes, the latter of which precondition the environment for moist convection and regulate the mesoscale flow dynamics. In recent decades, numerous studies have addressed this link in detail.

The present review article is not the first to cover the subject of orographic clouds and precipitation. Existing reviews and textbook chapters on this subject include, among others, Smith ([11] Chapter 4), Banta [12], Houze ([7] Chapter 12), Roe [13], Lin ([14] Chapter 11), Houze [15], and Colle et al. [16]. In contrast to those articles, which each encompassed a broad spectrum of orographic precipitation processes, this article provides a more compact and detailed review of the moist-convection sub-problem. Moreover, of the references just cited, only Banta [12] comprehensively addressed thermally forced orographic convection. Given the nearly 30 years that have since elapsed, an updated review incorporating more recent progress is needed. The present discussion is further restricted to moist convection that is locally initiated by orography, rather than the impacts of orography on preexisting convective systems, which was recently examined by Houze [15].

2. Background

This section briefly reviews two themes central to moist orographic convection: moist static instability and mountain airflow dynamics. Although each topic is covered extensively in the literature, this section provides vital context for the discussions of orographic convection to follow. For ease of reference, the term "moist orographic convection" is henceforth shortened to "orographic convection". In contrast, "dry convection" is not shortened.

2.1. Moist Static Instability

A moist-unstable atmosphere is one where saturated air parcels, when displaced vertically, accelerate away from their initial position. Because, to first order, temperature (T) controls buoyancy

at a given pressure (P), traditional static-stability analyses compare T of an adiabatically lifted parcel, drawn from some level or layer of the environment, to that of the undisturbed environment at the same P (e.g., [17]). Although accounting for water vapor and condensate by using density temperature (T_ρ) would be more accurate, our discussion keeps with tradition by using T. Layers where the parcel lapse rate ($\Gamma = -\partial T_p/\partial z$, where "p" refers to parcel) is less than that of the environment ($\gamma = -\partial T_e/\partial z$, where "e" refers to environment) are statically unstable because lifted air parcels become positively buoyant and thus accelerate upward. In contrast, layers with $\Gamma > \gamma$ are statically stable because lifted parcels become negatively buoyant and accelerate downward, and layers with $\Gamma = \gamma$ are statically neutral because lifted parcels are neither positively nor negatively buoyant.

When lifted, unsaturated parcels cool at the dry adiabatic lapse rate $\Gamma_d \approx g/c_p$ (≈ 9.8 K km^{-1}), where g is gravity and c_p is the specific heat of dry air at constant pressure. In contrast, saturated parcels undergo condensation and latent-heat release, and thus cool at the smaller saturated adiabatic lapse rate (Γ_s). Because the specific humidity of saturated air depends strongly on T, so does Γ_s; it decreases in warmer air due to increased latent-heat release. By comparing the parcel lapse rate to the environmental lapse rate, six different stability states can be defined: (i) absolutely stable ($\gamma < \Gamma_s$), (ii) saturated neutral ($\gamma_s = \Gamma_s$), (iii) conditionally unstable ($\Gamma_s < \gamma < \Gamma_d$), (iv) saturated absolutely unstable ($\gamma_s > \Gamma_s$), (v) dry neutral ($\gamma = \Gamma_d$), and (vi) dry absolutely unstable ($\gamma > \Gamma_d$), where γ and γ_s respectively correspond to the lapse rates of unsaturated and saturated environments [18].

In layers that satisfy criterion (iv) for conditional instability, sufficient moisture and/or forced lifting are also required to realize the instability. To account for these constraints, hypothetical parcel lifting profiles are often constructed. In the example of Figure 1, a surface-based parcel is lifted at a lapse rate of Γ_d until reaching saturation at the lifting condensation level (LCL), where its lapse rate transitions to Γ_s. If the environment at or above the LCL is conditionally unstable, continued lifting may allow the parcel to become warmer than it, and thus positively buoyant. The height where this occurs, if at all, is called the level of free convection (LFC). The parcel continues rising at Γ_s until its buoyancy returns to zero at the level of neutral buoyancy (LNB). The integrated buoyancy between the LFC and LNB is termed the convective available potential energy (CAPE), and the integrated negative buoyancy below the parcel's level of origin and the LFC (or the LNB, as the definition may vary) is termed the convective inhibition (CIN). For a surface-based parcel drawn from the sounding in Figure 1, CAPE = 1550 J kg^{-1} and CIN = 18 J kg^{-1}.

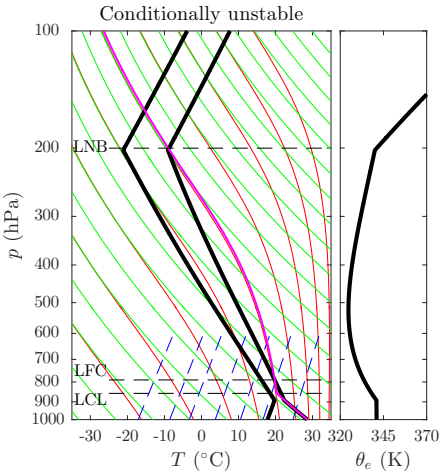

Figure 1. **Left**: skew-T/log-P diagram of a conditionally unstable environment [thick black lines show environmental T (right) and dewpoint T_d (left)]. Green lines are dry adiabats, red lines are moist adiabats, dashed blue lines correspond to T_d profiles of air with different saturation mixing ratios, and the thick magenta line is the path of an adiabatically lifted surface-based parcel. **Right**: corresponding profile of θ_e. The environment is dry neutral up to 900 hPa and conditionally and potentially unstable from 900 to ~500 hPa.

Potential instability, loosely defined as $\partial\theta_e/\partial z < 0$, relates to the lifting of an entire air layer (e.g., the entire sub-crest flow ascending a mountain) rather than an isolated parcel. When such a layer is brought to saturation, it becomes absolutely unstable in a parcel sense. As in Figure 1, conditional and potential instability often coexist. However, Figure 2 shows an example of an initial sounding that is potentially, but not conditionally, unstable. It exhibits a large decrease in relative humidity, and $\partial\theta_e/\partial z < 0$, over the 900–700 hPa layer (left two panels). When subject to an upward displacement of $\Delta z(p)$, part of this layer becomes saturated and absolutely unstable (right two panels). For a parcel drawn from the base of the lifted sounding, CAPE = 111 J kg^{-1} and CIN = 0 J kg^{-1}.

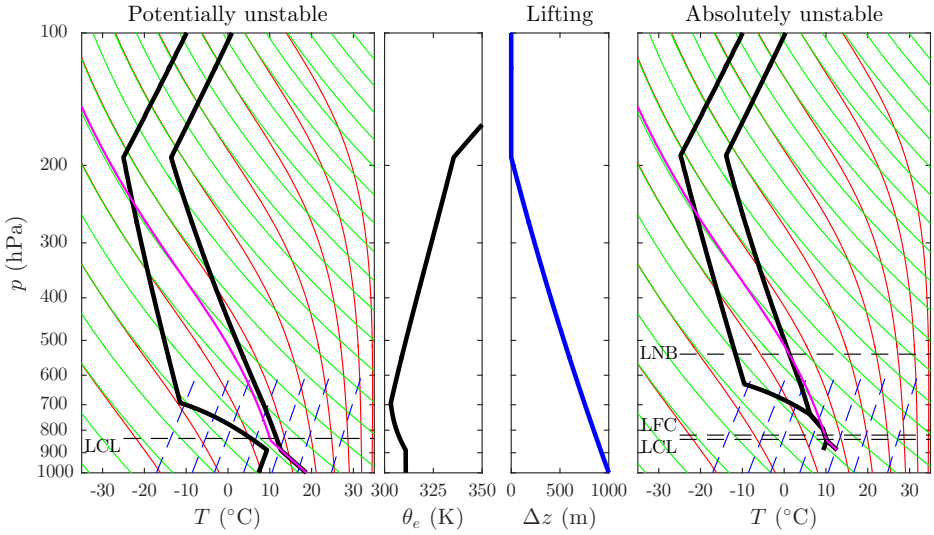

Figure 2. Left two panels: as in Figure 1, but for an initially absolutely stable and potentially unstable environment. Right two panels: through lifting by $\Delta z(p)$, the ~800–700 hPa layer becomes absolutely unstable.

2.2. Mountain Airflow Dynamics

2.2.1. Mechanically Forced Flows

In the absence of thermal forcing, impinging flow responds to mesoscale terrain by either ascending it or detouring around it. For a continuously stratified, adiabatic, and steady-state flow with uniform basic-state winds, this response is determined by two parameters: the nondimensional mountain height ($M = Nh_m/U$), where N is the Brunt-Väisälä frequency, h_m is the mountain height, and U is the cross-barrier wind speed, and the terrain aspect ratio ($r = a_y/a_x$), where a_x and a_y are the terrain length scales in the cross- and along-barrier directions [19]. Traditionally, both M and its reciprocal, the so-called mountain Froude number (Fr_m), have been used interchangeably to describe mountain flow regimes. However, because M has a straightforward interpretation as a nonlinearity parameter, while Fr_m is not a Froude number in the strictest sense (i.e. a ratio of fluid inertia to gravity-wave phase speed), the former is used herein to avoid confusion.

For $M > 1$ and $r \gtrsim 1$, the impinging flow tends to split upstream of the mountain and deflect around it ("blocked" flow), causing horizontal convergence near the upstream separation point and also downstream where the split airstreams rejoin. At steady state, upstream blocking extends over a distance of approximately $\min(a_y, L_d)$, where L_d is the Rossby radius of deformation [20]. If mountain wave breaking occurs aloft (favored for $1 < M < 2$ and $r > 1$), a decelerated wake may form in the lee with stagnant or even reversed flow. For $M \lesssim 1$ and/or $r << 1$, the flow tends to directly ascend the terrain ("unblocked" flow), with surface-based ascent over the windward slope. As a result, convective initiation tends to be focused upstream and/or downstream of the orography in blocked flow and over

the windward slopes in unblocked flow. Generally, unblocked flows experience larger near-surface vertical displacements than blocked flows, where displacements are roughly limited to U/N [21,22].

While M was originally derived for single-layer flows, it can in principle be reformulated for more complex vertical profiles of N and U by solving multi-layer linear wave equations. In practice, however, most studies applying M to such flows simply average N and U over the subcrest layer (e.g., [23]). Other complexities stem from diabatic processes, namely surface heating (e.g., [24–26]) and terrain-forced saturation and latent-heat release (e.g., [27,28]). Such heating locally reduces N (and, hence, M), which facilitates terrain-forced ascent. We henceforth refer to the "effective" M as the hypothetical value of M that accounts for such diabatic effects. Note also that most flows with $M \gtrsim 1$ are only partially blocked, with near-surface layers detouring around the mountain and elevated layers ascending it.

2.2.2. Thermally Forced Flows

Diabatic surface heating or cooling over mountainous terrain gives rise to thermally direct circulations. During the daytime, thermally driven surface-based flows of progressively larger horizontal scales (upslope, up-valley, and plain-to-mountain flows) ascend the terrain. These flows are primarily driven by buoyancy (upslope/anabatic flows) or by pressure gradient forces induced quasi-hydrostatically by thermal perturbations over the heated terrain (up-valley and plain-to-mountain flows) (e.g., [29]). Return flows aloft and thermally direct vertical motions form the remaining branches of these solenoidal circulations. Figure 3 provides a conceptual sketch of a daytime thermally forced circulation from Demko and Geerts [30], consisting of two up-mountain flows converging at the mountain crest to form a cumulus cloud.

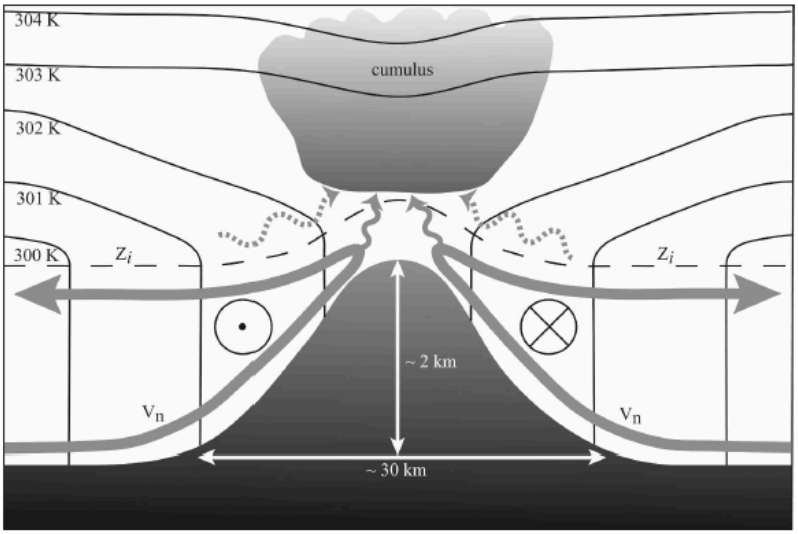

Figure 3. Schematic diagram of the low-level flow (v_n) associated with a thermally forced daytime solenoidal circulation over a mesoscale mountain from Demko and Geerts [30]. Thin solid lines are isentropes, horizontal vorticity is shown as vectors into and out of the page, and z_i denotes the ABL top. The cumulus cloud is fed in part by the solenoidal circulation and in part by horizontal convergence above the ABL.

Similarly, katabatic flows of increasing scale (downslope, down-valley, and mountain-to-plain) develop at night due to a reversal of the buoyancy (downslope/katabatic flows) and pressure-gradient (down-valley and mountain-to-plain flows) forces. Unlike the elevated ascent that occurs during the daytime, surface-based horizontal convergence and associated ABL ascent is focused at lower elevations surrounding the orography.

2.2.3. Parameters Controlling the Dominant Forcing

Whether an orographic flow is driven by mechanical and/or thermal forcing is central to interpreting the physics of convective initiation. Various nondimensional parameters comparing thermal to mechanical forcing amplitudes have been derived using linear theory [25,31,32], thermodynamic heat-engine theory [32–35], or scaling the pressure perturbations arising from each forcing [26,36]. Although the assumptions underlying each derivation varies, they all broadly agree that the role of thermal forcing is maximized for light background winds and weak low-level stability. Under these conditions, surface-based buoyancy anomalies can develop over the mountains without being readily ventilated downwind by the background flow, and large vertical displacements penetrating into the free troposphere are required to neutralize these anomalies.

Based on observations over the Vosges Mountains of southeastern France from the Convectively induced Orographic Precipitation (COPS) experiment in 2007, Hagen [37] found that M adequately distinguished between thermally and mechanically forced daytime convection. For $M > 1$, upstream blocking prevailed and solenoidal thermal circulations developed over the mountain ridge, promoting convective initiation near the crest. By contrast, for $M < 1$ the impinging flow crossed the Vosges, and convection developed when this flow converged with moist Rhine Valley air in the lee. Similarly, in trade-wind flow over the mountainous Caribbean island of Dominica during the Dominica Experiment (DOMEX) in 2011, Nugent et al. [38] found that the transition between thermally and mechanically forced convection largely depended on trade-wind flow speed (U), in part through its control over M. The former dominated for $U \lesssim 5$ m s^{-1} and the latter dominated for larger U.

Kirshbaum [26], however, cautioned that M is a flawed predictor of mountain flow regimes in the presence of thermal forcing. They found that a generalized M accounting for multi-layer flow (e.g., a convective ABL topped by an inversion), along with a thermal forcing parameter, were required to construct a regime diagram for diurnally heated orographic flows.

2.2.4. Interactions between Mechanical and Thermal Responses

When both mechanical and thermal forcing are active, the combined response differs from that associated with either forcing alone. For example, in mechanically unblocked or partially blocked flows with strong insolation, a warm thermal wake may develop in the mountain lee. The temperature gradient between the wake and its cooler surroundings gives rise to longitudinal convergence bands similar to sea-breeze convergence lines. If the mechanical response also exhibits lee-side convergence, such as the rejoining of split low-level airstreams, these two responses may superpose to strengthen lee ascent (e.g., [22,39,40]).

The combined response exhibits a diurnal cycle, as exemplified by trade-wind flow over the island of Hawaii, the peaks of which (∼4 km) pierce the nominal trade-wind inversion (1–3 km). Numerical simulations by Yang and Chen [41] indicate a nighttime flow with upstream blocking, downslope flow over the high terrain, and lee vortices in the mountain wake (Figure 4b). In the afternoon, the flow becomes unblocked with a strong lee flow reversal (Figure 4a). This diurnal oscillation of the mountain flow regime is consistent with the theory and idealized simulations of Reisner and Smolarkiewicz [25] and Kirshbaum [26], where sufficient thermal forcing was capable of eliminating upstream blocking and inducing lee-side upslope flow for $M > 1$.

Based on observational analysis of summertime airflows over Colorado, Banta [42] described another mechanism by which thermal and mechanical responses may interact. In the conceptual diagram of Figure 5, thermally driven lee-side upslope flow develops in the morning below a nocturnal inversion, which is decoupled from the overlying free troposphere. This easterly flow collides with westerly downslope flow to generate strong lee-side updrafts capable of initiating cumulus convection. In the afternoon, convective mixing recouples these two layers, eliminating the lee flow reversal.

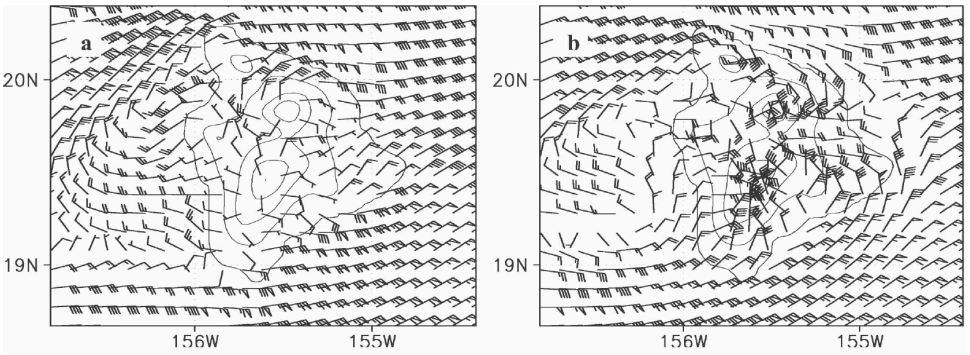

Figure 4. Time-averaged surface winds for a long-term simulation of trade-wind flow over Hawaii at (**a**) 1400 and (**b**) 0200 Hawaiian Solar Time (HST), from Yang and Chen [41]. Pennants, full barbs, and half barbs represent 5, 1, and 0.5 m s^{-1}, respectively. ©American Meteorological Society. Used with permission.

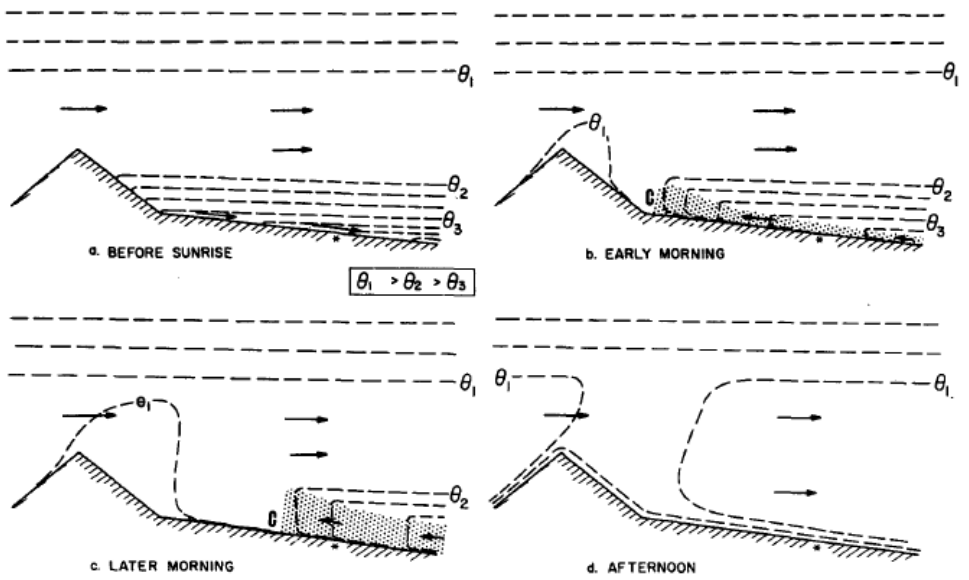

Figure 5. Schematic of diurnal flow development in the lee of a heated mountain, from Banta [42]. The cross-sections show potential temperature (θ) and cross-barrier winds in the: (**a**) nighttime, where both the ambient flow and sub-inversion flows are westerly, (**b**) early morning, where a shallow layer of easterly upslope flow develops below the inversion, (**c**) later morning, where the upslope flow deepens but is advected downstream by the background flow, and (**d**) the afternoon, where convective mixing eliminates the inversion and upslope flow. ©American Meteorological Society. Used with permission

3. Preconditioning

Building on the discussion of Section 2.1, two necessary and sufficient conditions for moist convection to occur at a given location are

1. CIN must locally equal zero, or sufficient forced lifting must be provided to overcome it,
2. CAPE must be sufficient for ascending cloudy thermals to overcome adverse processes that mitigate cloud development.

The "adverse processes" in item 2 above include entrainment (turbulent ingestion of environmental air), which reduces cloud buoyancy through dilution and evaporative cooling, and vertical pressure perturbations, which generally oppose the buoyancy force (e.g., [43]).

While Section 4 focuses on the dynamical "trigger" mechanisms needed to satisfy item 1 when CIN > 0, the present section focuses on the processes that precondition the local environment for convection, mainly by reducing CIN and/or enhancing CAPE.

3.1. Mechanically Forced Convection

In mechanically forced flows, the preconditioning for orographic convection relates to static destabilization and/or humidification of the impinging flow. Relevant preconditioning processes include large-scale ascent and advection, surface heating, and mesoscale differential advection. Because the former falls outside the scope of this article, we focus exclusively on the latter two processes.

Surface heating, realized through positive sensible- and/or latent-heat fluxes, increases the moist entropy (or, similarly, θ_e) of the ABL, which tends to reduce CIN and increase the tropospheric potential instability and CAPE. The diurnal cycle of these parameters, with larger (smaller) CAPE and smaller (larger) CIN in the daytime (nighttime), favors convective initiation during the daytime. Sensible heating tends to deepen the ABL and erode low-level temperature inversions. The resulting dry static destabilization and reduced M weakens upstream blocking and enhances terrain-forced ascent [26]. This destabilization further promotes convective initiation by reducing ABL CIN. However, ABL warming and buoyancy-driven mixing with the dry free troposphere can also suppress convection by reducing ABL relative humidity and CAPE [44].

Surface latent-heat fluxes promote deep convection by humidifying and facilitating saturation of the impinging flow, thus reducing the effective M and strengthening surface-based orographic ascent. Also, by enriching the ABL with moist-static energy, they reduce CIN and increase CAPE, which promotes and intensifies orographic convection (e.g., [45]). However, for a given solar energy input, increased latent-heat fluxes generally imply smaller sensible heat fluxes. If the latter are too small to erode stable layers suppressing convection, no amount of the former can ensure convective initiation. Similarly, if latent heat fluxes are minimal, the drying caused by pure sensible heating may inhibit convection. Hence, a favorable combination of both sensible and latent heating is needed to produce sufficient dry and moist static destabilization for convective initiation.

Orographic flows may be effectively preconditioned by traversing a warm water body prior to landfall. In the midlatitudes, this process is particularly important during autumn and winter where the residual heat content of large water bodies gives rise to sharp land–sea temperature contrasts. Strong onshore flows driven by midlatitude synoptic disturbances gain θ_e over the water surface, then readily develop convection when subsequently lifted by coastal terrain or land breezes. For example, along the coastal mountains of Washington and Oregon States (USA), precipitating shallow convection occurs regularly in the cold season following cold-frontal passage. The polar air behind these fronts is destabilized and moistened by the relatively warm ocean surface, and develops moist convection after landfall over the coastal mountains (e.g., [46]).

The Mediterranean Sea also preconditions orographic flows over southern Europe, the Middle East, and North Africa. Duffourg and Ducrocq [47] found that, for 10 high-precipitation events (HPEs) over the French Mediterranean region in autumn 2008–2009, evaporation over the Mediterranean accounted for a large fraction of the impinging low-level moisture content (∼30–70%), with larger fractions during anticyclonic large-scale conditions. Using numerical sensitivity experiments, Lebeaupin et al. [45] found that larger sea-surface temperatures (SSTs) intensified convection in such HPEs, while smaller SSTs weakened or even eliminated it. Similarly, in a numerical study of the 1994 Italy Piedmont flood, Buzzi et al. [28] found that larger SSTs enhanced convective precipitation over the coastal Appenines mountains but only minimally impacted the stratiform Alpine precipitation farther downstream.

Khodayar et al. [48] studied the climatology of atmospheric conditions associated with autumn HPEs in the western Mediterranean region. The most intense events featured abnormally large integrated water-vapor transport and CAPE in the upstream flow, and also reached maximum intensity during the afternoon, coinciding with the diurnal CAPE maximum. Several HPE hotspots were

identified along the windward slopes of regional orographic features, suggesting that terrain-forced lifting of onshore, synoptically driven flow was critical for initiating convection and/or enhancing larger-scale precipitation.

Another preconditioning mechanism is orographically induced differential advection within baroclinic flows. Smith [49] hypothesized that, when impinging cold fronts are blocked by tall orography, they may bend or fracture aloft, allowing progressively colder air aloft to override the blocked sub-crest flow. This process may ultimately give rise to a conditionally or absolutely unstable air column over the windward slope, within which moist convection may develop. Steenburgh [50] cited the potential importance of differential advection in an extreme snowstorm over the Wasatch Mountains of Utah, where layers of low θ_e aloft overrode surface-based layers of larger θ_e to promote heavy convective snowfall.

3.2. Thermally Forced Convection

In mechanically forced flows, the presence of upstream potential instability provides a useful (though not infallible) guideline for whether convection will occur if/when the flow is brought to saturation. This approach is less valid for thermally forced convection, where elevated heating, local thermal circulations, and vertical mixing may cause properties of the mountain atmosphere (including θ_e) to strongly differ from those in the surrounding flow (e.g., [51]). For example, in their analysis of Corsican deep convection during the Hydrologic Cycle in the Mediterranean (HyMeX) field campaign in 2012, Adler et al. [52] found that upstream soundings were insufficient to explain island convective initiation—local information on moist stability over the island terrain was also essential. Furthermore, the layer-lifting argument central to potential instability is less relevant to thermally forced circulations, which only lift near-surface air parcels to saturation (e.g., Figure 3). Thus, parcel-based stability metrics, namely the spatial distributions of CAPE and CIN, are generally more relevant to this problem.

The protrusion of mountains above low-level stable layers may facilitate thermally forced convection over high terrain. At night, katabatic flows drain radiatively cooled air into valleys and surrounding plains, inhibiting inversion formation over the peaks. As a consequence, CIN in the morning and early afternoon tends to exhibit local minima over the peaks. During IOP8b of COPS, where an isolated afternoon thunderstorm developed over the Black Forest Mountains of Germany, Behrendt et al. [53] found that CIN was generally smaller over Black Forest sites than over surrounding regions in the morning and early afternoon. Although the CIN minimum was located over the northern Black Forest, the thunderstorm developed over the southern Black Forest where locally stronger forcing for ascent coincided with low CIN. Such reduced CIN over the higher terrain was a consistent feature during COPS and helped to explain a higher frequency of convective initiation over the higher terrain [51].

Similarly, in a case study of diurnally forced deep convection over the Santa Catalina Mountains of southeast Arizona during the 2006 Cumulus Photogrammetric, In Situ, and Doppler Observations (CuPIDO) field campaign, Demko and Geerts [10] concluded that convection initiation was promoted by elevated destabilization over the high terrain. This conclusion was based on the mountain ABL extending above the nominal LFC from a sounding taken over surrounding low terrain. Although this interpretation is uncertain given the spatial heterogeneity of thermodynamic conditions over complex terrain, it still suggests that, as in COPS, reduced CIN over the higher terrain facilitated orographic convection in CuPIDO.

The above-mentioned protrusion of mountains into the nominal free troposphere also regulates ABL moisture supply. Because specific humidity generally decreases rapidly with height, environmental air over mountain ridges tends to be much drier than that near sea level. To humidify such regions, local surface evaporation and advection of moisture from lower levels is required. Adler and Kalthoff [54] observed processes regulating the atmospheric moisture supply over the mountainous Mediterranean island of Corsica during HyMeX. They found that the air over local terrain peaks tended to be more humid than that over surrounding regions during the day, suggesting the importance of

evapotranspiration and vertical transport of low-level moisture by thermal circulations. This moisture was then ventilated vertically by the mesoscale thermal circulations and buoyancy-driven turbulent mixing. Similarly, using radar and GPS data during COPS, Baelen et al. [55] observed a buildup of water vapor over the mountain crests prior to thermally driven convection events.

Another contribution to the boundary-layer humidity maximum, and thus convective initiation, over high terrain may stem from ABL entrainment processes. In semi-idealized simulations of flow over a flat, differentially heated surface, Garcia-Carreras et al. [56] found that thermally forced updrafts, which developed along gradients in land use, had larger θ_e than their surroundings. They attributed this finding to reduced entrainment of free-tropospheric air into the updrafts. A similar mechanism may give rise to local θ_e maxima within thermally forced mountain updrafts.

Orographic convection, particularly the thermally forced type, may also depend on soil moisture. For all else equal, wetter soils induce stronger moist destabilization but drier soils force stronger subcloud thermal circulations and more energetic ABL thermals. While the various interactions between soil moisture and convective precipitation have received extensive attention (more than sufficient for a separate review paper), we briefly review these interactions in the limited context of orographic convection. In monthlong explicit-convection simulations over the Alpine region, Hohenegger et al. [57] found a negative feedback between soil moisture and convective precipitation, as increased subcloud forcing over drier soils overwhelmed the increased moist destabilization over moister soils. By contrast, Zhou and Geerts [58] observed a positive correlation between soil moisture and summer monsoonal convection during the CuPIDO period. In addition, initial-value sensitivity tests of COPS events using numerical weather prediction (NWP) models have revealed a complex and non-monotonic sensitivity of orographic precipitation to soil moisture (e.g., [59,60]).

The idealized simulations of Imamovic et al. [61] suggest that sensitivity of orographic convection to soil moisture depends on the heterogeneity of the soil-moisture perturbations and h_m. For horizontally uniform soil-moisture variations, a positive sensitivity of convective precipitation to soil moisture was found, regardless of mountain height. However, when the soil-moisture variations were restricted to the mountain region, a negative sensitivity of local precipitation to soil moisture was found over shorter mountains ($h_m \leq 250$ m), similar to Hohenegger et al. [57]. However, this sensitivity vanished when h_m was increased to 500 m, suggesting that terrain-induced forcing may dominate the soil-moisture sensitivity over sufficiently tall mountains.

3.3. Orographic Impacts on Supercell Storm Environments

Regardless of the dominant forcing type, low-level flow perturbations induced by orography alter the thermodynamic conditions and winds of the storm environment. While a comprehensive discussion of the impacts of orography on preexisting convective systems falls outside the scope of this article, we briefly discuss the effect of orography on local supercell thunderstorm development. In an observational analysis of supercell-splitting events over central Switzerland, Houze et al. [62] noted that low-level orographic wind perturbations, by modifying directional wind shear, may favor either the right- or left-moving supercell. In idealized simulations of right-moving supercells traversing orography, Markowski and Dotzek [63] found that orographic modifications in relative humidity and convective inhibition substantially affected storm evolution, mainly by suppressing the supercells in downslope lee flow. Some supercells that survived into the lee exhibited a brief enhancement in low-level rotation if they propagated over a cyclonic lee vortex. Other studies of mountain convection have found that enhanced lee-side vertical shear, owing to thermally induced plain-to-mountain flow, can promote supercell formation and/or maintenance [64,65].

4. Trigger Mechanisms

In conditionally unstable environments with nonzero CIN (e.g., Figure 1), or in potentially unstable environments (e.g., Figure 2), finite-amplitude ascent is required to initiate moist convection. Both mechanical and thermal forcing can effectively produce such ascent, and this section overviews a

few common examples of each. For a more comprehensive list of precipitation mechanisms for both stratiform and convective clouds, we refer the reader to Houze [15].

4.1. Mechanical

4.1.1. Direct Orographic Ascent

Arguably the simplest mechanism of orographic convection is terrain-forced ascent in unblocked flow (Figure 6a). It requires that some streamlines are forcibly displaced to their LFC or higher, or that a potentially unstable layer is brought to saturation. Convection initiates near the point along the slope where the impinging flow first breaches its LFC. For $h_m >> LFC$, this occurs over the lower windward slopes, leading to convective precipitation enhancements well upstream of the mountain crest. In their study of Mediterranean HPEs, Khodayar et al. [48] found that the largest precipitation rates tended to occur at intermediate heights (300–1500 m) below the mountain tops, suggesting that these events were characterized by low CIN and $h_m > LFC$. Similarly, the radar analysis of Houze et al. [66] found that Alpine precipitation was maximized over the lower windward slopes in unblocked flow. For $h_m \approx LFC$, convective precipitation occurs closer to crest level. Due to strong descent, depletion of moisture, and mountain-wave-induced vertical mixing, this convection often dissipates rapidly in the lee [67,68].

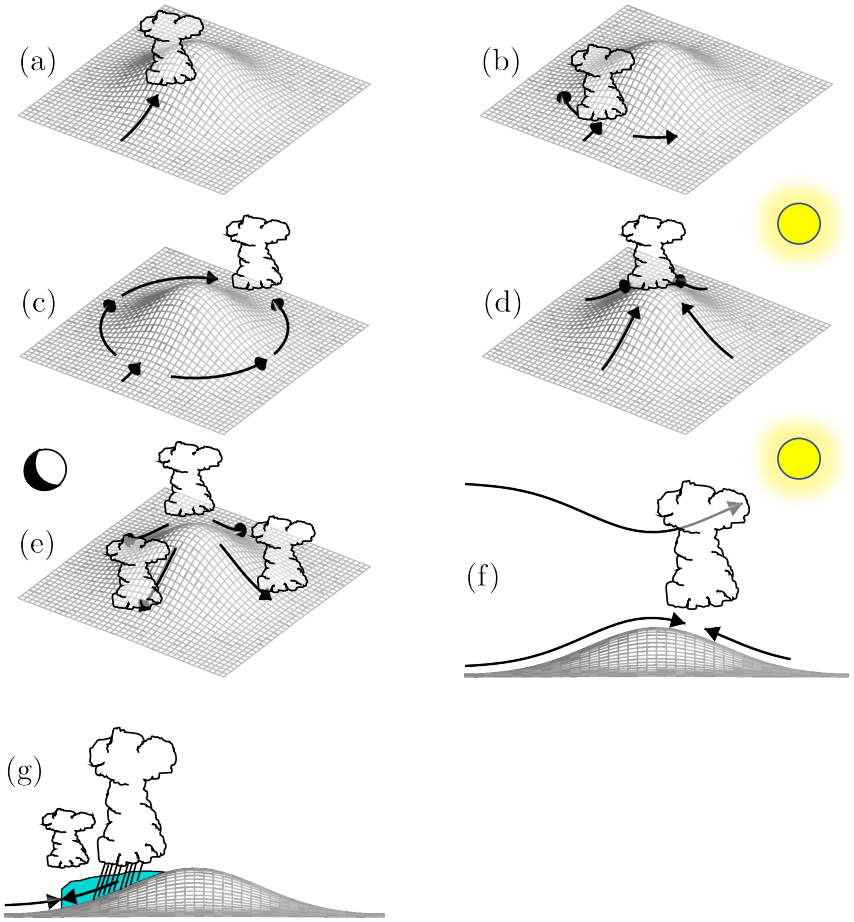

Figure 6. Schematic of basic mechanisms of convective initiation over mountains: (**a**) forced ascent, (**b**) upstream blocking, (**c**) lee-side convergence, (**d**) thermally forced anabatic flow and convection over the crest, (**e**) nocturnal katabatic flow and convection near the mountain base, (**f**) lee-side thermally driven upslope flow and gravity-wave ascent aloft, (**g**) quasi-stationary cold pool beneath precipitating convection.

Due to the simplicity and frequent occurrence of this trigger mechanism, it has received extensive attention. It prevails in conditionally unstable trade-wind flow when the terrain crest lies below the trade-wind inversion. This condition is frequently met over the smaller islands of Hawaii, such as Kauai (e.g., [69]) and Caribbean islands like Martinique and Dominica [4]. It is also associated with post-frontal convection over the Pacific Northwest USA [46] and in precipitation events in the Mediterranean and Alpine region (e.g., [48,70–72]).

In their idealized simulations of shallow, cellular orographic convection over a y-parallel ridge, Kirshbaum and Durran [6] and Fuhrer and Schär [73] found that stronger moist instability, larger cloud-layer depth, and larger-amplitude random perturbations in the upstream flow all increased the intensity of this convection. For convection to reach full intensity, it was found that the "advective" time scale for flow to traverse the mountain ($\sim a_x/U$) must exceed the "convective" time scale for unstable thermals to ascend through the cloud layer ($\sim z_{\mathrm{cld}}/w^*$, where z_{cld} and w^* are the cloud-layer depth and vertical-velocity scale) [74].

Further physical insights were provided by the large-eddy simulations of Dominican trade-wind convection by Kirshbaum and Smith [67]. They found that convective cells over the narrow island were more intense than corresponding cells over the upstream ocean, despite forming beneath a plunging trade-wind inversion. This island cloud invigoration apparently stemmed from the different lapse rates of dry and moist air parcels that were bodily lifted by the terrain—when lifted alongside unsaturated air, the island clouds attained larger buoyancies than the clouds over the surrounding ocean. Kirshbaum and Grant [75] found that such orographically forced convective cells also had larger cross-sectional horizontal areas than corresponding cells over the ocean, which mitigated the suppressive effects of entrainment.

Organized convective precipitation bands over windward slopes have also been variously observed (e.g., [44,46,76,77]). These features may become quasi-stationary and concentrate heavy precipitation over preferred locations. For example, in a banded convection event over the Oregon Coastal Range, Kirshbaum and Durran [46] found that cumulative precipitation over an 8-h period varied from 69 mm directly underneath a band (at Mt. Hebo) to only 3 mm about 20 km farther up the slope (at Rye Mountain) (Figure 7). Such bands remain anchored in place due to persistent updrafts associated with standing lee waves and/or surface-based convergence zones past small-scale topographic features [78–81].

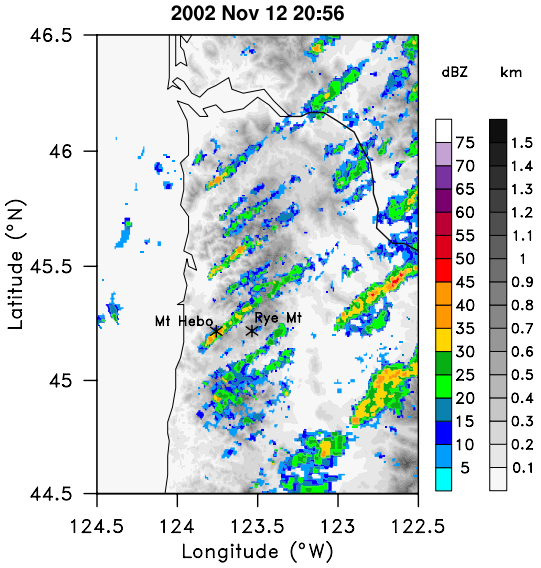

Figure 7. Snapshot of radar reflectivity (color fill) atop Oregon Coastal Range terrain (gray fill) at 20:56 UTC on 12 November 2002, showing organized convective rainbands in postfrontal flow. This same case was studied in detail by Kirshbaum and Durran [46] and Kirshbaum et al. [79].

4.1.2. Upstream Blocking

In blocked flows with $M \gtrsim 1$, convection may be initiated by horizontal deceleration and convergence upstream of the barrier (Figure 6b). Studies of this process include Grossman and Durran [82], who observed monsoonal convection upstream of the Western Ghats Mountains of India. Along with quantifying the upstream deceleration and associated convergence that forced convective initiation, they also noted that strong descent over the mountain tops suppressed convection there. Similarly, in a radar climatology over the Alps, Houze et al. [66] found that in large-M flow, upstream blocking caused convective precipitation enhancements to shift well upstream of the barrier, relative to that in unblocked flow. A well-observed case of such upstream-shifted convection occurred during IOP8 of the 1999 Mesoscale Alpine Programme (MAP) field campaign. The combination of forced ascent over coastal terrain and upstream blocking by the Alps led to heavy convective precipitation over coastal regions far upstream of the Alps [83,84]. A similar event was observed over northeastern Italy during HyMeX [85], where low-level blocking gave rise to an Alpine barrier jet that induced convective initiation well upstream of the Alps.

4.1.3. Lee-Side Convergence

Impinging airstreams with $M \gtrsim 1$ that split and detour laterally around terrain edges may rejoin in the lee to produce sufficient ascent for convective initiation (Figure 6c). While some debate has centered on whether such flow is actually convergent or just confluent [12], various studies have suggested the importance of this mechanism. For example, Mass [86] documented lee-side convergence past the Olympics Mountains of Washington State, which regularly focuses banded convection over the downstream Puget Sound region. A similar mechanism was also hypothesized to generate quasi-stationary convection events downstream of the UK Lake District [87] and Corsica during HyMeX [88,89].

4.1.4. Mountain Waves

Vertically propagating mountain waves also produce updrafts that may regulate moist convection. Along with forced, surface-based ascent of low-level flow (as described in Section 4.1.1 and represented in Figure 6a), elevated updrafts associated with these waves form directly above or downwind of the mountain, centered at a height of approximately one vertical wavelength above the surface. Based on linear theory of steady, 2D, Boussinesq flow with uniform N and U, such waves only develop when the Fourier terrain spectrum contains forcing at scales satisfying $k < N/U$, where k is the horizontal wavenumber (e.g., [90]). Over smaller features with $k > N/U$, the waves are evanescent. In the hydrostatic limit, the vertical wavelength is $\lambda_z = 2\pi U/N$. Elevated mountain-wave updrafts can, in principle, initiate elevated convection or invigorate convective systems propagating through them. However, while various studies have speculated on the importance of these waves for moist convection (e.g., [15,34,91]), few have presented convincing evidence of it. This may stem from the high altitude of elevated updrafts: for a hypothetical flow with $U = 10$ m s^{-1} and $N = 0.01$ s^{-1}, $\lambda_z = 6.3$ km. Generally, the source layers of moist convection are based lower in the troposphere.

Breaking mountain waves may also generate surface-based hydraulic jumps in the lee. In single-layer hydraulic flow, these jumps develop when subcritical flow (Froude number $Fr = U/\sqrt{gH} < 1$, where g is gravitational acceleration and H is the fluid depth) transitions to supercritical ($Fr > 1$) over an obstacle. Durran [90] and Smith et al. [92] define effective Fr for analogous atmospheric configurations. In neutrally stratified cross-barrier flow capped by a strong inversion, g and H may be replaced by the effective gravity ($g' = \Delta\theta/\theta_0$), where $\Delta\theta$ is the potential-temperature jump across the inversion and θ_0 is the sub-inversion potential temperature) and the depth of the layer below the inversion, respectively [92]. A hydraulic jump represents a sharp boundary between strong downslope flow and decelerated or reversed wake flow, with locally strong horizontal convergence and intense updrafts. If the wake flow is conditionally unstable, convection may be

initiated along the hydraulic jump. Bhushan and Barros [93] noted the importance of hydraulic jumps for convective initiation in simulations of deep convection over central Mexico during a major monsoonal precipitation event. Moreover, in idealized simulations of squall lines crossing a ridge, Frame and Markowski [94] found that, as the cold pool from a squall line descends the lee slope, it may develop a hydraulic jump that regenerates the squall line in the lee.

4.2. Thermal

4.2.1. Daytime Flows

Upslope flows, up-valley flows, and plain-to-mountain flows produce ascending air currents along insolated mountain faces. As up-mountain flows from different sides of the mountain converge near or downwind of mountain crest, they give rise to strong updrafts that penetrate into the free troposphere and effectively initiate moist convection (Figure 6d). As a result, summer convection climatologies generally exhibit hot spots over and just downwind of prominent mountain crests (e.g., [95–97]). Even modest terrain features of a few hundred meters or less relief (e.g., the Palmer Divide of central Colorado or the Turtle Plateau of North Dakota) may produce sufficient ABL horizontal convergence to noticeably increase the frequency of convection initiation.

From aircraft transects over the Santa Catalina mountains of Arizona, Braham and Draginis [98] observed a daytime "convective core" over the high terrain, consisting of upslope flow along the ridge slopes and a strong updraft over the mountaintop that initiated shallow cumuli (qualitatively similar to that shown in Figure 3). Further observational evidence of such convective cores was obtained over New Mexico by Raymond and Wilkening [99,100]. Similar circulations were also obtained in early idealized numerical models with parameterized surface heating and turbulent mixing [101,102].

Although the convective core provides a vital forcing for convective initiation, other circulations (both orogenic and synoptic) can also play important roles. In their numerical case-study of diurnal convection events over the Black Forest, Barthlott et al. [103] noted the importance of organized valley flows (within the Kinzig, Rench, and Murg valleys) for concentrating horizontal convergence and cumulus convection. A variety of thermally forced orographic convection events were also observed during the CuPIDO (e.g., [10,30,104,105]), COPS (e.g., [53,106–108]), and DOMEX [35,38,109] field campaigns. Interestingly, the COPS IOP8b isolated convection event was hypothesized to involve not one but two convergence zones: one a quasi-stationary thermally forced updraft over the Black Forest, and the other a propagating, synoptically driven convergence zone that crossed the Black Forest. The thunderstorm appeared to develop when these two convergence zones briefly superposed [110]. However, Behrendt et al. [53] concluded that the thermally driven wind system over the Black Forest, along with locally reduced CIN, was alone sufficient for convective initiation in this event.

4.2.2. Nighttime Flows

Katabatic, down-valley, and mountain-to-plain flows driven by nocturnal cooling over higher terrain can initiate convection when they converge with ambient flows near the mountain base (Figure 6e). Such flows are generally less effective at initiating convection than corresponding daytime flows because of the stronger static stability of the nocturnal ABL, which restricts vertical motion and limits surface-based moist instability. Nevertheless, observations over orographic regions indicate a diurnal oscillation in the convection maximum, transitioning from a primary afternoon maximum over the high terrain to a secondary maximum over surrounding areas at night (e.g., [88,111–117]).

The importance of katabatic flows relative to other forcing mechanisms for nocturnal convection remains unclear, as the coexistence of multiple such mechanisms complicates the picture. These other mechanisms include (i) land breezes [112,118], (ii) offshore-propagation gravity waves caused by either daytime ABL heating [113,119] or deep moist convection over elevated terrain [120], (iii) advection of elevated moisture perturbations by the background flow [111,114], and (iv) elevated potential vorticity anomalies caused by elevated diurnal heating drifting downwind to initiate convection [121].

The relative importance of each above mechanism may depend on various parameters, including topography (both terrain and land cover), latitude, heating amplitude, and environmental conditions. Reports of events where katabatic forcing appeared particularly instrumental for nocturnal convection include Barthlott et al. [88], who studied two cases of nocturnal convection near Corsica. In one case, deep convection formed to the east of Corsica, due to a combination of a land breeze and katabatic drainage flows induced by the island's steep terrain. The katabatic flow was necessary to produce a sufficiently deep layer of offshore flow to initiate convection as it converged with ambient southeasterly winds. In addition, Mazón and Pino [122] concluded that katabatic winds played a key role in numerous nocturnal convection events offshore of the Iberian Peninsula, and Yu and Jou [123] reached a similar conclusion about nocturnal convection offshore of Taiwan.

4.2.3. Combined Mechanical and Thermal Forcing

As discussed in Section 2.2.4, the combination of mechanical and thermal forcing can lead to stronger orographically induced ascent than that from either source alone. One such example is the aforementioned lee-side convergence mechanism of Banta [42], where unblocked flow converges with decoupled, thermally driven upslope flow in the lee (Figure 5). Because unblocked flows also tend to develop vertically propagating mountain waves, surface-based updrafts driven by this mechanism may align with elevated wave updrafts, extending the surface-based ascent over a deep layer (Figure 6f). Such alignment of lee-side updrafts within different layers occurred in the large-eddy simulations of Kirshbaum ([26] their Figure 4d), and is thought to contribute to summertime deep convection downstream of the Colorado Rockies [91].

Another such mechanism, also discussed in Section 2.2.4, is the combination of mechanically and thermally driven convergence within or downwind of a mountain wake. Barrett et al. [87] studied a UK precipitation event where a quasi-stationary convective band developed downwind of the Lake District in a flow with $M > 1$. In their numerical simulations of the event, both forcing sources were required to produce sufficient lee-side convergence to anchor the band (their Figure 16). Similarly, Yang et al. [39] found that mechanically and thermally forced convergence aligned in the wake of Kauai and Niihau islands over Hawaii to generate long cloud bands in the lee. Such island "cloud trails" were also studied in detail by Kirshbaum and Fairman [40] over the Lesser Antilles.

Kirshbaum [124] and Metzger et al. [125] examined the sensitivity of midlatitude orographic convection to the upstream wind speed and direction. They found that, as in Nugent et al. [38], the flow regime transitions from thermally to mechanically forced as the upstream wind speed is increased, which impacts local thermodynamic conditions and the amplitude and position of low-level updrafts. Weaker winds, or winds aligned with the main axis of the terrain, favored deep convection by (i) enhancing the static destabilization of the mountain atmosphere and (ii) facilitating strong, thermally forced updrafts over the high terrain. Stronger winds weakened the low-level convergence and shifted it downstream of the crest, which reduced the forcing for ascent and the vigor of the resulting convection.

4.2.4. Diabatic Feedbacks

When cumulonimbi develop over a mountain range, evaporative cooling of falling precipitation may give rise to subcloud cold pools. Because such cold pools are negatively buoyant, they tend to accelerate downhill. As shown by idealized simulations of mechanically forced convection over simple ridges [126–128], the evolution of such convection depends on the relation between cold-pool upstream propagation speed and the background wind speed. When the former exceeds the latter, the cold pool propagates upstream, leading to an upstream propagation of the convective system and a cessation of convection over the ridge. In contrast, when the winds exceed the cold-pool propagation speed, the cold pool propagates downstream, leading to the formation of two systems: a quasi-stationary convective system over the ridge and a downstream-propagating disturbance forced by the cold pool.

The leading edge of the cold pool may also remain quasi-stationary upstream of the ridge crest (as depicted in Figure 6g). Based on idealized numerical simulations of conditionally unstable flow over a quasi-2D ridge, Miglietta and Rotunno [129] found that the most favorable environmental configuration for this scenario is a vertically reverse-sheared cross-barrier flow, with strong impinging flow near the surface and weak flow aloft. This combination enabled the cross-barrier low-level flow to just balance the upstream cold-pool propagation, while the orographically forced convection remained quasi-stationary due to the weak winds aloft. Moreover, consistent with the theory of Rotunno et al. [130] for long-lived squall lines, the horizontal vorticity of the ambient wind profile balanced the baroclinic vorticity of the cold pool, promoting a deep and upright surface-based updraft at the cold pool's leading edge. This favorable regime for long-lived and intense orographic convection is consistent with conditions during real-case HPEs including the 1974 Oahu flood [131], the 1976 Colorado Big Thompson flood [132], and the Gard flood in southern France [71].

A related mechanism was proposed by Soderholm et al. [64] to explain the development of quasi-stationary deep convection in thermally forced orographic convection events over the Black Hills mountains of South Dakota and Wyoming (USA). Under unidirectional cross-barrier winds, cold pools produced by orographic cumulonimbi descend the lee slope to cut off the lee-side anabatic flow required for convective initiation, leading to a pause or cessation of the convection (Figure 8a,c) (e.g., [10,58,124]). However, if the low-level winds are aligned parallel to the ridge, they can separate the cold pool from the along-ridge convergence line, allowing cumulonimbi to repeatedly develop along the ridge with little interference from the cold pools (Figure 8b,d).

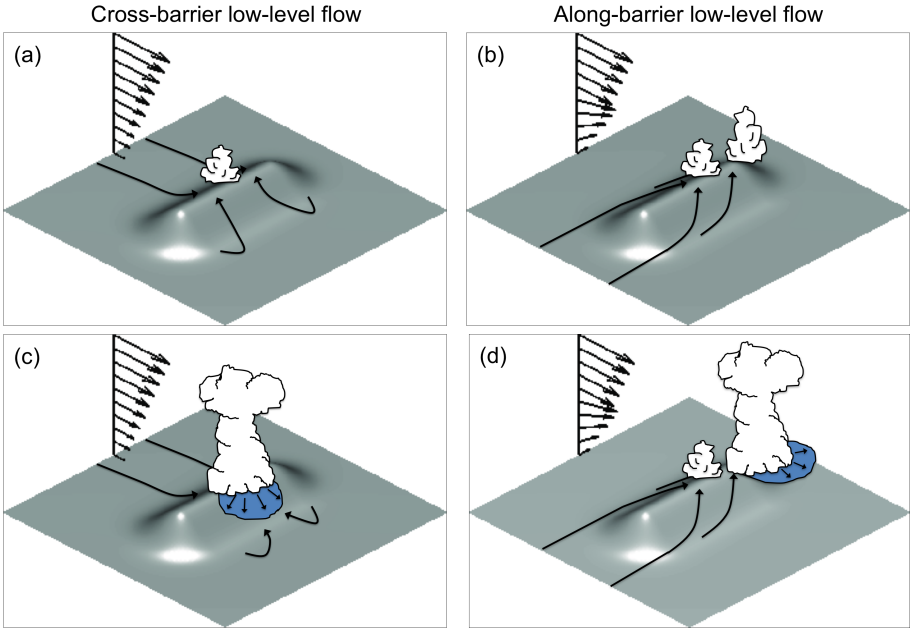

Figure 8. Schematic of the role of low-level winds on deep-convective evolution over a heated ridge, from Soderholm et al. [64]. For cross-barrier low-level winds (**a**) and (**c**), windward flow converges with reversed lee-side flow over or downwind of the crest, producing strong updrafts. Cumulonimbi thus initiated create cold pools that cut off the lee upslope flow and thus weaken the elevated convergence. For along-barrier low-level winds (**b**) and (**d**), the flow is drawn upslope as it parallels the ridge, again creating a convergence line along the crest. Cumulonimbi thus initiated create cold pools that propagate downwind and do not weaken the elevated convergence.

When thermally induced circulations give rise to orographic cumuli, the associated latent-heat release may reinforce the thermal circulation by locally enhancing low-level pressure gradients. However, the resulting cloud shading may produce a negative feedback by locally reducing the

insolation. Using systematic numerical sensitivity experiments, Wang and Kirshbaum [35] quantified these two effects for a case of thermally forced shallow convection during DOMEX. While the former effect enhanced the onshore flow feeding the circulation by ∼20%, the cloud shading weakened it by a similar amount. As a result, the overall thermal circulation was minimally affected by cloud formation over the island.

5. Summary and Outlook

This article has reviewed the physical mechanisms underlying moist orographic convection, including both preconditioning and triggering, along with the connections between these mechanisms and surface-exchange processes. The discussion focused on research over the 2–3 decades since the comprehensive review article of Banta [12] on orographic clouds and precipitation. Progress over this time has been accelerated by multiple observational field campaigns over various regions, along with complementary modelling and theoretical studies. To organize this discussion, we decomposed the basic problem of moist orographic convection according to the dominant mechanism responsible for orographic ascent: mechanical versus thermal forcing. The former corresponds to the flow of impinging air over or around an orographic barrier and the latter corresponds to thermally forced circulations driven by differential heating over complex terrain.

5.1. Outstanding Challenges

Despite the above-mentioned progress, uncertainties and knowledge gaps continue to limit conceptual understanding and model prediction of orographic convection. Such limitations are inevitable given the highly complex, nonlinear, and multi-scale nature of the relevant processes. Nevertheless, these issues can and should be addressed through concerted research efforts that exploit technological advancements in atmospheric observation and modelling.

The understanding of mechanically forced convection benefits from a strong theoretical foundation of mountain airflow dynamics rooted in steady-state linear theory. However, numerous outstanding questions pertain to nonlinear and/or transient processes, such as cloud-diabatic feedbacks on mountain airflow, preconditioning by upstream surface heat fluxes, ABL and in-cloud turbulence, and cloud-microphysical processes. For example, when an entire ABL is lifted to saturation over a mountain, the resulting cloud dynamics are intricately tied to turbulent processes within the impinging ABL. Fully understanding the former demands an adequate characterization of the latter. A particularly important parameter for this convection is the relative humidity of the impinging flow, which regulates both the amplitude of terrain-forced ascent (by controlling windward saturation) and the intensity of the resulting convection.

For thermally forced convection, physical understanding is further challenged by the essential nonlinearity of thermally driven circulations [32], large spatial heterogeneity in thermodynamics and winds over and across complex terrain, and multi-scale interactions between the land surface and the ABL. As a result, the dynamics of thermally forced mountain circulations, and the thermodynamic conditions of the air within these circulations, remain poorly understood. In fact, even the roles of basic terrain scales (e.g., a_x and h_m, in 2D flow) on thermally forced convection remain uncertain. Different theoretical frameworks (e.g., linear theory and heat-engine theory) predict different sensitivities of thermal-updraft strength to these scales [32], which calls for additional numerical experimentation to resolve such discrepancies. Moreover, the strength of subcloud updrafts is only one factor regulating convection initiation—local thermodynamic conditions, the source regions of the ascending air, mid-tropospheric humidity, etc., are also important.

The above gaps in knowledge must be addressed not only to gain insight into meteorologically significant processes, but also to improve convection parameterization schemes in NWP and climate models. Most such schemes adopt a mass-flux approach (e.g., [133]), where the subgrid convection is assumed to consist of an ensemble of plumes in convective quasi-equilibrium [134]. The upward mass flux at cloud base constitutes the "closure", and the set of criteria that determine where and

when convection is activated is termed the "trigger function". The sensitivity of parameterized convection to the formulation of the convective trigger [135] and closure [136] are well established. However, a longstanding deficiency in these schemes has been the absence of a physically-based parameterization for the impacts of subcloud orographic forcing [137].

5.2. Building a Better Understanding

5.2.1. Observations

High-quality, high-resolution, and comprehensive atmospheric measurements are needed to gain new insights into the above issues. Emeis et al. [138] provide a comprehensive overview about the state-of-the-art measurement systems and their potential for future field studies. We limit the present discussion to addressing the potential of available instruments for studying moist orographic convection and outlining some basic measurement considerations that should be taken into account before conducting relevant field campaigns.

Firstly, atmospheric conditions and processes must be measured over an appropriate range of scales. To this end, the investigation area, instrumentation, and scanning strategies must be chosen appropriately. For instance, in thermally forced flow, the mesoscale solenoidal circulations, their embedded turbulent eddies, and surface exchange processes must be simultaneously resolved to quantify the contribution of each process to the evolution of parameters relevant for moist convection. Secondly, measurements deficits, which derive from previous investigations, should be considered. For example, Khodayar et al. [139] found that the multi-scale spatial distribution of water vapor and low-level wind convergence over complex terrain during a HyMeX event was adequately resolved by regional operational networks inland but not over the adjacent sea, where the spatiotemporal resolution of observation platforms was insufficient to identify conditions relevant for convection. Thirdly, new measurement techniques should be exploited.

To adequately observe orographic convection events, high-resolution measurements of surface energy exchange, spatial distributions of heat, moisture and momentum, and cloud development are needed. This requires dense networks of surface-energy stations, along with vertical profilers of temperature, humidity and 3D winds at different locations (valley, slopes, ridges, and plateaus). The latter may use a combination of in situ and remote sensing instruments, including radiosondes, sodars, ultra-high-frequency (UHF) wind profilers, and Doppler LiDARs. Airborne LiDAR and radar measurements are needed for spatial information on winds and clouds. By positioning Doppler LiDARs in valleys, slopes, and ridges, dual and triple Doppler wind analyses can be performed to retrieve high-resolution spatial wind fields. Accurate wind retrievals at high temporal resolution can be achieved by applying the virtual tower technique or co-planar scans [140].

Additional information on the crucially important water-vapor field over complex terrain can be provided by microwave radiometers (e.g., [54]) and by integrated water vapor from GPS networks [52,141]. Wind LiDARs and water vapor differential absorption LiDARs (DIALs) can be combined to determine latent heat flux profiles, particularly at sites of specific interest for ABL evolution. Precipitation radars at elevated sites with undisturbed views of the horizon are needed to continuously monitor precipitation. These data can be combined with precipitation data from mobile communication networks [142] as well as lightning data, which serve as a proxy for deep convection (e.g., [88]). As access to commercial microwave link networks becomes easier, completely new options to retrieve precipitation information become available (e.g., [142,143]). Scanning cloud radars positioned at hot spots prone to convection initiation, along with high-resolution satellite data like NASA's new GOES-R satellite, should be used to monitor the early, non-precipitating stages of incipient cloud evolution.

Comprehensive observation platforms, both fixed [144,145] and mobile [146], have recently been designed to provide high-quality data sets on land-surface exchange processes, convection, and cloud

and precipitation evolution over limited areas. Such platforms should be increasingly utilized to complement operational and other special observing facilities in future field campaigns.

Beyond observational field campaigns, the utility of satellites for climatological monitoring of orographic convection will also increase. Along with new geostationary satellites with sub-kilometer spatial resolution (e.g., GOES-R), NASA's new Global Precipitation Measurement (GPM) mission provides 3D precipitation information over the globe with a spatial resolution of 5 km. Thus, studies along the lines of Romatschke and Houze [116,117], which previously were confined to lower latitudes (due to the limited coverage of NASA's Tropical Measurement Rainfall Measuring Mission satellite), can now be extended to the midlatitudes.

5.2.2. Numerical Simulations and Theory

Numerical models are essential for both the prediction and physical understanding of orographic convection. As computer power increases, more relevant processes can be explicitly represented through the use of finer model grids and/or larger domains. In principle, these advancements should enhance the predictive skill of NWP models over complex terrain. For example, the recent transition from convection-parameterizing [O (10 km)] to convection-permitting [O (1 km)] grid spacing in regional NWP models has improved the skill of summer precipitation forecasts over the Black Forest (e.g., [147]). An important follow-up question is whether additional improvements will arise through the transition from convection-permitting to eddy-resolving [O (100 m)] grids with explicit ABL turbulence and an improved representation of cumulus clouds (e.g., [148]).

Although higher grid resolution provides obvious benefits to NWP, it also raises new challenges. The predictability of orographic convection in such models is limited by uncertainties in their initial conditions (ICs) as well as model error. While finer grids can reduce model error by reducing the reliance on uncertain subgrid parameterization schemes, they induce faster error growth on the smaller, newly resolved scales [149], which can grow upscale to contaminate the larger-scale flow [150]. Thus, to realize the potential benefits of higher grid resolution on NWP forecasts, the initial amplitudes of small-scale IC errors must be held to a minimum. To this end, the assimilation of high-resolution remote observations (e.g., from radars, LiDARs, and satellites) becomes increasingly important. Such assimilation, however, is particularly challenging because thermal-wind balance, which usefully constrains mass and wind fields on the synoptic scale, breaks down on the mesoscale.

Improved NWP models also facilitate conceptual understanding by providing gridded, dynamically consistent, four-dimensional data sets of real-world events. As events of interest become more accurately represented, analyses of model data and hypothesis-testing sensitivity experiments can provide new insights into the key processes underlying them. Idealized simulations are also essential for systematically isolating and quantifying processes of interest in a simplified framework. Both of these experimental configurations are useful to explore new frontiers of domain size, grid resolution, and integration time, to determine optimal model configurations for representing orographic convection events. Moreover, simultaneous representation of a larger spectrum of processes permits a more seamless investigation of multi-scale process interactions.

Finally, an improved theoretical understanding of orographic convection is needed to parameterize related processes in NWP and (particularly) climate models. Recent studies have addressed this need by quantifying and scaling boundary-layer updrafts and mass fluxes [22,26,32,34,35] and cumulus entrainment [75] in orographic flows. However, no studies to date have addressed the difficult problem of orographic convection in the mountain "grey zone", where a smoothed profile of a mountain range is explicitly resolved but important smaller-scale forcing is not. Future studies must confront this challenge to develop scale-aware parameterizations of subgrid orographic triggering of convection.

Acknowledgments: The contributions of DJK were supported by funding from Natural Science and Engineering Research Council Grant (NSERC) grants RGPIN 418372-17 and RGPAS 507900-17. The authors are grateful to Mathias Rotach and Dino Zardi, who encouraged this submission, and to Christoph Schär, who provided helpful insights during the manuscript preparation.

Author Contributions: D.J.K. organized the paper, wrote most of the text, and prepared all figures. S.S., C.B., B.A., and N.K. provided valuable ideas, guidance with the presentation, and additional text. In particular, B.A. and N.K. contributed most of the text in Section 5.2.1, and S.S. contributed text to Sections 2.2.2, 5.1, and 5.2.2.

Conflicts of Interest: The authors declare no conflict of interest.

References

1. Frei, C.; Schär, C. A precipitation climatology of the Alps from high-resolution rain-gauge observations. *Int. J. Climatol.* **1998**, *18*, 873–900.
2. Smith, R.B.; Barstad, I.; Bonneau, L. Orographic precipitation and Oregon's climate transition. *J. Atmos. Sci.* **2005**, *62*, 177–191.
3. Daly, C.; Halbleib, M.; Smith, J.I.; Gibson, W.P.; Doggett, M.K.; Taylor, G.H.; Curtis, J.; Pasteris, P.P. Physiographically sensitive mapping of climatological temperature and precipitation across the conterminous United States. *Int. J. Climatol.* **2008**, *28*, 2031–2064.
4. Smith, R.B.; Schafer, P.; Kirshbaum, D.J.; Regina, E. Orographic precipitation in the tropics: Experiments in Dominica. *J. Atmos. Sci.* **2009**, *66*, 1698–1716.
5. Durran, D.R.; Klemp, J.B. On the effects of moisture on the Brunt-Väisälä frequency. *J. Atmos. Sci.* **1982**, *39*, 2152–2158.
6. Kirshbaum, D.J.; Durran, D.R. Factors governing cellular convection in orographic precipitation. *J. Atmos. Sci.* **2004**, *61*, 682–698.
7. Houze, R.A. *Cloud Dynamics*; Academic Press: Cambridge, MA, USA, 1993; 573p.
8. Bergeron, T. On the low level redistribution of atmospheric water caused by orography. In Proceedings of the International Conference on Cloud Physics, Tokyo and Sapporo-shi, Japan, 24 May–1 June 1965; pp. 96–100.
9. Bader, M.J.; Roach, W.T. Orographic rainfall in warm sectors of depressions. *Q. J. R. Meteorol. Soc.* **1977**, *103*, 269–280.
10. Demko, J.C.; Geerts, B. A numerical study of the evolving convective boundary layer and orographic circulation around the Santa Catalina Mountains in Arizona. Part II: Interaction with deep convection. *Mon. Weather Rev.* **2010**, doi:10.1175/2010MWR3318.1.
11. Smith, R.B. The influence of mountains on the atmosphere. *Adv. Geophys.* **1979**, *21*, 87–230.
12. Banta, R.M. The role of mountain flows in making clouds. In *Atmospheric Processes over Complex Terrain*; Meteorological Monographs; American Meteor Society: Boston, MA, USA, 1990; Volume 23, pp. 229–283.
13. Roe, G.H. Orographic precipitation. *Annu. Rev. Earth Planet. Sci.* **2005**, *33*, 645–671.
14. Lin, Y.L. *Mesoscale Dynamics*; Cambridge University Press: Cambridge, UK, 2007; 630p.
15. Houze, R.A. Orographic effects on precipitating clouds. *Rev. Geophys.* **2012**, *50*, RG1001.
16. Colle, B.A.; Smith, R.B.; Wesley, D.A. Theory, observations, and predictions of orographic precipitation. In *Mountain Weather Research and Forecasting: Recent Progress and Current Challenges*; Chow, F.K., De Wekker, S.F., Snyder, B.J., Eds.; Springer: Dordrecht, The Netherlands, 2013; pp. 291–344.
17. Saucier, W.J. *Principles of Meteorological Analysis*; University of Chicago Press: Chicago, IL, USA, 1955; 438p.
18. Bryan, G.H.; Fritsch, J.M. Moist absolute instability: The sixth static stability state. *Bull. Am. Meteorol. Soc.* **2000**, *81*, 1207–1230.
19. Smith, R.B. Hydrostatic flow over mountains. *Adv. Geophys.* **1989**, *31*, 1–41.
20. Pierrehumbert, R.T.; Wyman, B. Upstream effects of mesoscale mountains. *J. Atmos. Sci.* **1985**. 977–1003.
21. Ólafsson, H.; Bougeault, P. The effect of rotation and surface friction on orographic drag. *J. Atmos. Sci.* **1997**, *54*, 193–210.
22. Kirshbaum, D.J.; Wang, C.C. Boundary layer updrafts driven by airflow over heated terrain. *J. Atmos. Sci.* **2014**, *71*, 1425–1442.
23. Reinecke, P.A.; Durran, D.R. Estimating topographic blocking using a Froude number when the static stability Is nonuniform. *J. Atmos. Sci.* **2008**, *65*, 1035–1048.

24. Raymond, D.J. Calculation of airflow over an arbitrary ridge including diabatic heating and cooling. *J. Atmos. Sci.* **1972**, *29*, 837–843.
25. Reisner, J.M.; Smolarkiewicz, P.K. Thermally forced low Froude number flow past three-dimensional obstacles. *J. Atmos. Sci.* **1994**, *51*, 117–133.
26. Kirshbaum, D.J. On upstream blocking over heated mountain ridges. *Q. J. R. Meteorol. Soc.* **2017**, *143*, 53–68.
27. Davies, H.; Schär, C. Diabatic modification of airflow over a mesoscale orographic ridge: A model study of the coupled response. *Q. J. R. Meteorol. Soc.* **1986**, *112*, 711–730.
28. Buzzi, A.; Tartaglione, N.; Malguzzi, P. Numerical simulations of the 1994 Piedmont flood: Role of orography and moist processes. *Mon. Weather Rev.* **1998**, *126*, 2369–2383.
29. Zardi, D.; Whiteman, C.D. Diurnal mountain wind systems. In *Mountain Weather Research and Forecasting: Recent Progress and Current Challenges*; Chow, F.K., De Wekker, S.F., Snyder, B.J., Eds.; Springer: Dordrecht, The Netherlands, 2013; pp. 35–119.
30. Demko, J.C.; Geerts, B. Boundary layer energy transport and cumulus development over a heated mountain: An observational study. *Mon. Weather Rev.* **2009**, *137*, 447–468.
31. Crook, N.A.; Tucker, D.F. Flow over heated terrain. Part I: Linear theory and idealized numerical simulations. *Mon. Weather Rev.* **2005**, *133*, 2552–2564.
32. Kirshbaum, D.J. On thermally forced circulations over heated terrain. *J. Atmos. Sci.* **2013**, *70*, 1690–1709.
33. Souza, E.P.; Renno, N.O.; Dias, M.A.F.S. Convective circulations induced by surface heterogeneities. *J. Atmos. Sci.* **2000**, *57*, 2915–2922.
34. Tian, W.S.; Parker, D.J. A modeling study and scaling analysis of orographic effects on boundary layer shallow convection. *J. Atmos. Sci.* **2003**, *60*, 1981–1991.
35. Wang, C.C.; Kirshbaum, D.J. Thermally forced convection over a mountainous tropical island. *J. Atmos. Sci.* **2015**, *72*, 2484–2506.
36. Lewis, H.W.; Mobbs, S.D.; Vosper, S.B.; Brown, A.R. The effect of surface heating on hill-induced flow separation. *Bound. Layer Meteorol.* **2008**, *129*, 269–287.
37. Hagen, M.; van Baelen, J.; Richard, E. Influence of the wind profile on the initiation of convection in mountainous terrain. *Q. J. R. Meteorol. Soc.* **2011**, *137*, 224–235.
38. Nugent, A.D.; Smith, R.B.; Minder, J.R. Wind speed control of tropical convection. *J. Atmos. Sci.* **2014**, *71*, 2695–2711.
39. Yang, Y.; Xie, S.P.; Hafner, J. The thermal wake of Kauai island: Satellite observations and numerical simulations. *J. Clim.* **2008**, *21*, 4568–4586.
40. Kirshbaum, D.J.; Fairman, J.G., Jr. Cloud trails past the Lesser Antilles. *Mon. Weather Rev.* **2015**, *143*, 1425–1442.
41. Yang, Y.; Chen, Y.L. Effects of terrain heights and sizes on island-scale circulations and rainfall for the island of Hawaii during HaRP. *Mon. Weather Rev.* **2008**, *136*, 120–146.
42. Banta, R.M. Daytime boundary-layer evolution over mountainous terrain. Part I: Observations of the dry circulations. *Mon. Weather Rev.* **1984**, *112*, 340–356.
43. Markowski, P.; Richardson, Y. *Mesoscale Meteorology in Midlatitudes*; Wiley: Hoboken, NJ, USA, 2010; 430p.
44. Miller, D.K. Near-term effects of the lower atmosphere in simulated northwest flow snowfall forced over the southern Appalachians. *Weather Forecast.* **2012**, *27*, 1198–1216.
45. Lebeaupin, C.; Ducrocq, V.; Giordani, H. Sensitivity of torrential rain events to the sea surface temperature based on high-resolution numerical forecasts. *J. Geophys. Res. Atmos.* **2006**, *111*, D12110.
46. Kirshbaum, D.J.; Durran, D.R. Observations and modeling of banded orographic convection. *J. Atmos. Sci.* **2005**, *62*, 1463–1479.
47. Duffourg, F.; Ducrocq, V. Origin of the moisture feeding the heavy precipitating systems over southeastern France. *Nat. Hazard Earth Syst.* **2011**, *11*, 1163–1178.
48. Khodayar, S.; Kalthoff, N.; Kottmeier, C. Atmospheric conditions associated with heavy precipitation events in comparison to seasonal means in the western Mediterranean region. *Clim. Dyn.* **2016**, 1–17, doi:10.1007/s00382-016-3058-y.
49. Smith, R.B. A differential model of thermal advection. *Mon. Weather Rev.* **1982**, *110*, 306–309.
50. Steenburgh, W.J. One hundred inches in one hundred hours: Evolution of a Wasatch Mountain winter storm cycle. *Weather Forecast.* **2003**, *18*, 1018–1036.

51. Kalthoff, N.; Kohler, M.; Barthlott, C.; Adler, B.; Mobbs, S.D.; Corsmeier, U.; Traumner, K.; Foken, T.; Eigenmann, R.; Krauss, L.; et al. The dependence of convection-related parameters on surface and boundary-layer conditions over complex terrain. *Q. J. R. Meteorol. Soc.* **2011**, *137*, 70–80.
52. Adler, B.; Kalthoff, N.; Kohler, M.; Handwerker, J.; Wieser, A.; Corsmeier, U.; Kottmeier, C.; Lambert, D.; Bock, O. The variability of water vapour and pre-convective conditions over the mountainous island of Corsica. *Q. J. R. Meteorol. Soc.* **2016**, *142*, 335–346.
53. Behrendt, A.; Pal, S.; Aoshima, F.; Bender, M.; Blyth, A.; Corsmeier, U.; Cuesta, J.; Dick, G.; Dorninger, M.; Flamant, C.; et al. Observation of convection initiation processes with a suite of state-of-the-art research instruments during COPS IOP 8b. *Q. J. R. Meteorol. Soc.* **2011**, *137*, 81–100.
54. Adler, B.; Kalthoff, N. Multi-scale transport processes observed in the boundary layer over a mountainous island. *Bound. Layer Meteorol.* **2014**, *153*, 515–537.
55. van Baelen, J.; Reverdy, M.; Trido, F.; Labbouz, L.; Dick, G.; Bender, M.; Hagen, M. On the relationship between water vapour field evolution and the life cycle of precipitation systems. *Q. J. R. Meteorol. Soc.* **2011**, *137*, 204–223.
56. Garcia-Carreras, L.; Parker, D.J.; Marsham, J.H. What is the mechanism for the modification of convective cloud distributions by land surface-induced flows? *J. Atmos. Sci.* **2011**, *68*, 619–634.
57. Hohenegger, C.; Brockhaus, P.; Bretherton, C.S.; Schär, C. The soil moisture-precipitation feedback in simulations with explicit and parameterized convection. *J. Clim.* **2009**, *22*, 5003–5020.
58. Zhou, X.; Geerts, B. The influence of soil moisture on the planetary boundary layer and on cumulus convection over an isolated mountain. Part I: Observations. *Mon. Weather Rev.* **2013**, *141*, 1061–1078.
59. Hauck, C.; Barthlott, C.; Krauss, L.; Kalthoff, N. Soil moisture variability and its influence on convective precipitation over complex terrain. *Q. J. R. Meteorol. Soc.* **2011**, *137*, 161–175.
60. Barthlott, C.; Kalthoff, N. A numerical sensitivity study on the impact of soil moisture on convection-related parameters and convective precipitation over complex terrain. *J. Atmos. Sci.* **2011**, *68*, 2971–2987.
61. Imamovic, A.; Schlemmer, L.; Schär, C. Collective impacts of orography and soil moisture on the soil moisture-precipitation feedback. *Geophys. Res. Lett.* **2017**, *44*, doi:10.1002/2017GL075657.
62. Houze, R.A.; Schmid, W.; Fovell, R.G.; Schiesser, H.H. Hailstorms in Switzerland: Left movers, right movers, and false hooks. *Mon. Weather Rev.* **1993**, *121*, 3345–3370.
63. Markowski, P.; Dotzek, N. A numerical study of the effects of orography on supercells. *Atmos. Res.* **2011**, *100*, 457–478.
64. Soderholm, B.; Ronalds, B.; Kirshbaum, D.J. The evolution of convective storms initiated by an isolated mountain ridge. *Mon. Weather Rev.* **2014**, *142*, 1430–1451.
65. Scheffkneckt, P.; Serafin, S.; Grubisic, V. A long-lived supercell over mountainous terrain. *Q. J. R. Meteorol. Soc.* **2017**, *143*, 2973–2986.
66. Houze, R.A., Jr.; James, C.N.; Medina, S. Radar observations of precipitation and airflow on the Mediterranean side of the Alps: Autumn 1998 and 1999. *Q. J. R. Meteorol. Soc.* **2001**, *127*, 2537–2558.
67. Kirshbaum, D.J.; Smith, R.B. Orographic precipitation in the tropics: Large-eddy simulations and theory. *J. Atmos. Sci.* **2009**, *66*, 2559–2578.
68. Minder, J.; Smith, R.B.; Nugent, A.D. The dynamics of ascent-forced orographic convection in the tropics: results from Dominica. *J. Atmos. Sci.* **2013**, *70*, 4067–4088.
69. Ramage, C.S.; Schroeder, T.A. Trade wind rainfall atop Mount Waialeale, Kauai. *Mon. Weather Rev.* **1999**, *127*, 2217–2226.
70. Ascencio, N.; Stein, J.; Chong, M.; Gheusi, F. Analysis and simulation of local and regional conditions for the rainfall over the Lago Maggiore Target Area during MAP IOP 2b. *Q. J. R. Meteorol. Soc.* **2003**, *129*, 565–586.
71. Ducrocq, V.; Nuissier, O.; Ricard, D.; Lebeaupin, C.; Thouvenin, T. A numerical study of three catastrophic precipitating events over western Mediterranean region (southern France). Part II: Mesoscale triggering and stationarity factors. *Q. J. R. Meteorol. Soc.* **2008**, *134*, 131–145.
72. Röhner, L.; Nerding, K.N.; Corsmeier, U. Diagnostic study of a HyMeX heavy precipitation event over Spain by investigation of moisture trajectories. *Q. J. R. Meteorol. Soc.* **2016**, *142*, 287–297.
73. Fuhrer, O.; Schär, C. Embedded cellular convection in moist flow past topography. *J. Atmos. Sci.* **2005**, *62*, 2810–2828.
74. Cannon, D.J.; Kirshbaum, D.J.; Gray, S.L. Under what conditions does embedded convection enhance orographic precipitation? *Q. J. R. Meteorol. Soc.* **2012**, *138*, 391–406.

75. Kirshbaum, D.J.; Grant, A.L.M. Invigoration of cumulus cloud fields by mesoscale ascent. *Q. J. R. Meteorol. Soc.* **2012**, *138*, 2136–2150.
76. Miniscloux, F.; Creutin, J.D.; Anquetin, S. Geostatistical analysis of orographic rainbands. *J. Appl. Meteorol.* **2001**, *40*, 1835–1854.
77. Barrett, A.I.; Gray, S.L.; Kirshbaum, D.J.; Roberts, N.M.; Schultz, D.M.; Fairman, J.G., Jr. The utility of convection-permitting ensembles for the prediction of stationary convective bands. *Mon. Weather Rev.* **2016**, *144*, 1093–1114.
78. Cosma, S.; Richard, E.; Miniscloux, F. The role of small-scale orographic features in the spatial distribution of precipitation. *Q. J. R. Meteorol. Soc.* **2002**, *128*, 75–92.
79. Kirshbaum, D.J.; Bryan, G.H.; Rotunno, R.; Durran, D.R. The triggering of orographic rainbands by small-scale topography. *J. Atmos. Sci.* **2007**, *64*, 1530–1549.
80. Kirshbaum, D.J.; Rotunno, R.; Bryan, G.H. The spacing of orographic rainbands triggered by small-scale topography. *J. Atmos. Sci.* **2007**, *64*, 4222–4245.
81. Fuhrer, O.; Schär, C. Dynamics of orographically triggered banded convection in sheared moist orographic flows. *J. Atmos. Sci.* **2007**, *64*, 3542–3561.
82. Grossman, R.L.; Durran, D.R. Interaction of low-level flow with the western Ghat mountains and offshore convection in the summer monsoon. *Mon. Weather Rev.* **1984**, *112*, 652–672.
83. Bousquet, O.; Smull, B.F. Observations and impacts of upstream blocking during a widespread orographic precipitation event. *Q. J. R. Meteorol. Soc.* **2003**, *129*, 391–409.
84. Medina, S.; Houze, R.A. Air motions and precipitation growth in Alpine storms. *Q. J. R. Meteorol. Soc.* **2003**, *129*, 345–371.
85. Davolio, S.; Volonté, A.; Manzato, A.; Pucillo, A.; Sicogna, A.; Ferrario, M.E. Mechanisms producing different precipitation patterns over north-eastern Italy: Insights from HyMeX-SOP1 and previous events. *Q. J. R. Meteorol. Soc.* **2016**, *142*, 188–205.
86. Mass, C. Topographically forced convergence in western Washington state. *Mon. Weather Rev.* **1981**, *109*, 1335–1347.
87. Barrett, A.I.; Gray, S.L.; Kirshbaum, D.J.; Roberts, N.M.; Schultz, D.M.; Fairman, J.G., Jr. Synoptic versus orographic control on stationary convective banding. *Q. J. R. Meteorol. Soc.* **2015**, *141*, 1101–1113.
88. Barthlott, C.; Adler, B.; Kalthoff, N.; Handwerker, J.; Kohler, M.; Wieser, A. The role of Corsica in initiating nocturnal offshore convection. *Q. J. R. Meteorol. Soc.* **2016**, *142*, 222–237.
89. Scheffkneckt, P.; Richard, E.; Lambert, D. A highly localized high-precipitation event over Corsica. *Q. J. R. Meteorol. Soc.* **2016**, *142*, 206–221.
90. Durran, D.R. Mountain waves and downslope winds. In *Atmospheric Processes over Complex Terrain*; Meteorological Monographs; American Meteor Society: Boston, MA, USA, 1990; Volume 23, pp. 59–83.
91. Tripoli, G.J.; Cotton, W.R. Numerical study of an observed orogenic mesoscale convective system. Part I: Simulated genesis and comparison with observations. *Mon. Weather Rev.* **1989**, *117*, 273–304.
92. Smith, R.B.; Gleason, A.C.; Gluhosky, P.A.; Grubiŝić, V. The wake of St. Vincent. *J. Atmos. Sci.* **1997**, *54*, 606–623.
93. Bhushan, S.; Barros, A.P. A numerical study to investigate the relationship between moisture convergence patterns and orography in central Mexico. *J. Hydrometeorol.* **2007**, *8*, 1264–1284.
94. Frame, J.; Markowski, P. The interaction of simulated squall lines with idealized mountain ridges. *Mon. Weather Rev.* **2006**, *134*, 1919–1941.
95. Kuo, J.T.; Orville, H.D. A radar climatology of summertime convective clouds in the Black Hills. *J. Appl. Meteorol.* **1973**, *12*, 359–368.
96. Banta, R.M.; Schaaf, C.B. Thunderstorm genesis zones in the Colorado Rocky Mountains as determined by traceback of geosynchronous satellite images. *Mon. Weather Rev.* **1987**, *115*, 463–476.
97. Weckwerth, T.M.; Wilson, J.W.; Hagen, M.; Emerson, T.J.; Pinto, J.O.; Rife, D.L.; Grebe, L. Radar climatology of the COPS region. *Q. J. R. Meteorol. Soc.* **2011**, *137*, 31–41.
98. Braham, R.R., Jr.; Draginis, M. Roots of orographic cumuli. *J. Meteorol.* **1960**, *17*, 214–226.
99. Raymond, D.J.; Wilkening, M.H. Mountain-induced convection under fair weather conditions. *J. Atmos. Sci.* **1980**, *37*, 2693–2706.
100. Raymond, D.J.; Wilkening, M.H. Flow and mixing in New Mexico cumuli. *J. Atmos. Sci.* **1982**, *39*, 2211–2228.

101. Orville, H.D. A photogrammetric study of the initiation of cumulus clouds over mountainous terrain. *J. Atmos. Sci.* **1965**, *22*, 700–709.
102. Gal-Chen, T.; Somerville, R.C.J. Numerical solution of the Navier-Stokes equations with topography. *J. Comput. Phys.* **1975**, *17*, 276–310.
103. Barthlott, C.; Corsmeier, U.; Meissner, C.; Braun, F.; Kottmeier, C. The influence of mesoscale circulation systems on triggering convective cells over complex terrain. *Atmos. Res.* **2006**, *81*, 150–175.
104. Demko, J.C.; Geerts, B. A numerical study of the evolving convective boundary layer and orographic circulation around the Santa Catalina Mountains in Arizona. Part I: Circulation without deep convection. *Mon. Weather Rev.* **2010**, *138*, 1902–1922.
105. Zehnder, J.A.; Hu, J.; Radzan, A. Evolution of the vertical thermodynamic profile during the transition from shallow to deep convection during CuPIDO 2006. *Mon. Weather Rev.* **2009**, *137*, 937–953.
106. Kottmeier, C.; Kalthoff, N.; Barthlott, C.; Corsmeier, U.; van Baelen, J.; Behrendt, A.; Behrendt, R.; Blyth, A.; Coulter, R.; Crewell, S.; et al. Mechanisms initiating deep convection over complex terrain during COPS. *Meteorol. Z.* **2008**, *17*, 931–948.
107. Bennett, L.J.; Blyth, A.M.; Burton, R.R.; Gadian, A.M.; Weckwerth, T.M.; Behrendt, A.; Girolamo, P.D.; Dorninger, M.; Lock, S.J.; Smith, V.H.; et al. Initiation of convection over the Black Forest mountains during COPS IOP15a. *Q. J. R. Meteorol. Soc.* **2011**, *137*, 176–189.
108. Richard, E.; Chaboureau, J.P.; Flamant, C.; Champollion, C.; Hagen, M.; Schmidt, K.; Kiemle, C.; Corsmeier, U.; Barthlott, C.; Di Girolamo, P. Forecasting summer convection over the Black Forest: A case study from the Convective and Orographically-induced Precipitation Study (COPS) experiment. *Q. J. R. Meteorol. Soc.* **2011**, *137*, 101–117.
109. Smith, R.B.; Nugent, A.; Minder, J.; Kirshbaum, D.J.; Warren, R.; Lareau, N.; Palany, P.; James, A.; French, J. Orographic precipitation in the tropics: The Dominica Experiment. *Bull. Am. Meteorol. Soc.* **2012**, *93*, 1567–1579.
110. Kalthoff, N.; Adler, B.; Barthlott, C.; Corsmeier, U.; Mobbs, S.D.; Crewell, S.; Traumner, K.; Kottmeier, C.; Wieser, A.; Smith, V.; et al. The impact of convergence zones on the initiation of deep convection: A case study from COPS. *Atmos. Res.* **2009**, *93*, 680–694.
111. Hales, J.E., Jr. On the relationship of convective cooling to nocturnal thunderstorms at Phoenix. *Mon. Weather Rev.* **1977**, *105*, 1609–1613.
112. Houze, R.A., Jr.; Geotis, S.G.; Marks, F.D., Jr.; West, A.K. Winter monsoon convection in the vicinity of north Borneo. Part I: Structure and time variation of the clouds and precipitation. *Mon. Weather Rev.* **1981**, *109*, 1595–1614.
113. Mapes, B.E.; Warner, T.T.; Xu, M. Diurnal patterns of rainfall in northwestern South America: Part III. Diurnal gravity waves and nocturnal convection offshore. *MWR* **2003**, *131*, 830–844.
114. Sato, T.; Kimura, F. Diurnal cycle of convective instability around the central mountains in Japan during the warm season. *J. Atmos. Sci.* **2005**, *62*, 1626–1636.
115. Qian, J.H. Why precipitation is mostly concentrated over islands in the Maritime Continent. *J. Atmos. Sci.* **2009**, *65*, 1428–1441.
116. Romatschke, U.; Houze, R.A., Jr. Characteristics of precipitating convective systems in the South Asian monsoon. *J. Hydrometeorol.* **2011**, *12*, 3–26.
117. Romatschke, U.; Houze, R.A., Jr. Characteristics of precipitating convective systems in the premonsoon season of South Asia. *J. Hydrometeorol.* **2011**, *12*, 157–180.
118. Wapler, K.; Lane, T.P. A case of offshore convective initiation by interacting land breezes near Darwin, Australia. *Meteorol. Atmos. Phys.* **2012**, *115*, 123–137.
119. Li, Y.; Carbone, R.E. Offshore propagation of coastal precipitation. *J. Atmos. Sci.* **2015**, *72*, 4553–4568.
120. Hassim, M.E.; Lane, T.P.; Grabowski, W.W. The diurnal cycle of rainfall over New Guinea in convection-permitting WRF simulations. *Atmos. Chem. Phys.* **2016**, *16*, 161–175.
121. Li, Y.; Smith, R.B. The detection and significance of diurnal pressure and potential vorticity anomalies east of the Rockies. *J. Atmos. Sci.* **2010**, *67*, 2734–2751.
122. Mazón, J.; Pino, D. Nocturnal offshore precipitation near the Mediterranean coast of the Iberian Peninsula. *Meteorol. Atmos. Phys.* **2012**, *120*, 11–28.
123. Yu, C.K.; Jou, B.J.D. Radar observations of the diurnally forced offshore convective lines along the southeastern coast of Taiwan. *Mon. Weather Rev.* **2005**, *133*, 1613–1636.

124. Kirshbaum, D.J. Cloud-resolving simulations of deep convection over a heated mountain. *J. Atmos. Sci.* **2011**, *68*, 361–378.
125. Metzger, J.; Barthott, C.; Kalthoff, N. Impact of upstream flow conditions on the initiation of moist convection over the island of Corsica. *Atmos. Res.* **2014**, *145–146*, 279–296.
126. Chu, C.M.; Lin, Y.L. Effects of orography on the generation and propagation of mesoscale convective systems in a two-dimensional conditionally unstable flow. *J. Atmos. Sci.* **2000**, *57*, 3817–3837.
127. Chen, S.H.; Lin, Y.L. Effects of moist Froude number and CAPE on a conditionally unstable flow over a mesoscale mountain ridge. *J. Atmos. Sci.* **2005**, *62*, 331–350.
128. Miglietta, M.M.; Rotunno, R. Numerical simulations of conditionally unstable flows over a ridge. *J. Atmos. Sci.* **2009**, *66*, 1865–1885.
129. Miglietta, M.M.; Rotunno, R. Numerical simulations of sheared conditionally unstable flows over a mountain ridge. *J. Atmos. Sci.* **2014**, *71*, 1647–1662.
130. Rotunno, R.; Klemp, J.B.; Weisman, M.L. A theory for strong, long-lived squall lines. *J. Atmos. Sci.* **1988**, *45*, 463–485.
131. Schroeder, T.A. Meteorological analysis of an Oahu flood. *Mon. Weather Rev.* **1977**, *105*, 458–468.
132. Caraceña, F.R.; Maddox, R.A.; Hoxit, L.R.; Chappell, C.F. Mesoanalysis of the Big Thompson storm. *Mon. Weather Rev.* **1979**, *107*, 1–17.
133. Plant, R.S. A review of the theoretical basis for bulk mass flux convective parameterization. *Atmos. Chem. Phys.* **2010**, *10*, 3529–3544.
134. Yano, J.I.; Plant, R.S. Convective quasi-equilibrium. *Rev. Geophys.* **2012**, *50*, RG4004.
135. Kain, J.S.; Fritsch, J.M. The role of the convective "trigger function" in numerical forecasts of mesoscale convective systems. *Meteorol. Atmos. Phys.* **1992**, *49*, 93–106.
136. Bechtold, P.; Semane, N.; Lopez, P.; Chaboureau, J.P.; Beljaars, A.; Bormann, N. Representing Equilibrium and Nonequilibrium Convection in Large-Scale Models. *J. Atmos. Sci.* **2014**, *71*, 734–753.
137. Yano, J.I.; Geleyn, J.F.; Köhler, M.; Mironov, D.; Quaas, J.; Soares, P.M.M.; Phillips, V.T.J.; Plant, R.S.; Deluca, A.; Marquet, P.; et al. Basic Concepts for Convection Parameterization in Weather Forecast and Climate Models: COST Action ES0905 Final Report. *Atmosphere* **2015**, *6*, 88–147.
138. Emeis, S.; Kalthoff, N.; Adler, B.; Pardyiak, E.; Paci, A. High-resolution observation of transport and exchange processes in mountainous terrain. *Atmosphere*, submitted for publication, **2018**.
139. Khodayar, S.; Raff, F.; Kalthoff, N.; Bock, O. Diagnostic study of a high-precipitation event in the western Mediterranean: Adequacy of current operational networks. *Q. J. R. Meteorol. Soc.* **2016**, *142*, 72–85.
140. Stawiarski, C.; Träumner, K.; Knigge, C.; Calhoun, R. Scopes and challenges of dual-doppler Lidar wind measurements—An error analysis. *J. Atmos. Ocean. Tech.* **2013**, *30*, 2044–2062.
141. Khodayar, S.; Kalthoff, N.; Wickert, J.; Kottmeier, C.; Dorninger, M. High-resolution representation of the mechanisms responsible for the initiation of isolated thunderstorms over flat and complex terrains: Analysis of CSIP and COPS cases. *Meteorol. Atmos. Phys.* **2013**, *119*, 109–124.
142. Chwala, C.; Keis, F.; Kunstmann, H. Real-time data acquisition of commercial microwave link networks for hydrometeorological applications. *Atmos. Meas. Tech.* **2016**, *9*, 991–999.
143. Gosset, M.; Kunstmann, H.; Zougmore, F.; Cazenave, F.; Leijnse, H.; Uijlenhoet, R.; Chwala, C.; Keis, F.; Doumounia, A.; Boubacar, B.; et al. Improving rainfall measurement in gauge poor regions thanks to mobile telecommunication networks. *Bull. Am. Meteorol. Soc.* **2016**, *97*, ES49–ES51.
144. Bühl, J.; Seifert, P.; Wandinger, U.; Baars, H.; Thomas Kanitz, J.S.; Myagkov, A.; Engelmann, R.; Skupin, A.; Heese, B.; Klepel, A.; et al. LACROS: The Leipzig Aerosol and Cloud Remote Observations System. In Proceedings of the Spie Remote Sensing, Dresden, Germany, 23–26 September 2013.
145. Löhnert, U.; Schween, J.H.; Acquistapace, C.; Ebell, K.; Maahn, M.; Barrera-Verdejo, M.; Hirsikko, A.; Bohn, B.; Knaps, A.; O'Connor, E.; et al. JOYCE: Jülich Observatory for Cloud Evolution. *Bull. Am. Meteorol. Soc.* **2015**, *96*, 1157–1174.
146. Kalthoff, N.; Adler, B.; Wieser, A.; Kohler, M.; Träumner, K.; Handwerker, J.; Corsmeier, U.; Khodayar, S.; Lambert, D.; Kopmann, A.; et al. KITcube: A mobile observation platform for convection studies deployed during HyMeX. *Meteorol. Z.* **2013**, *22*, 633–647.
147. Schwitalla, T.; Bauer, H.S.; Wulfmeyer, V.; Zängl, G. Systematic errors of QPF in low-mountain regions as revealed by MM5 simulations. *Meteorol. Z.* **2008**, *17*, 903–919.

148. Panosetti, D.; Böing, S.; Schlemmer, L.; Schmidli, J. Idealized large-eddy and convection-resolving simulations of moist convection over mountainous terrain. *J. Atmos. Sci.* **2016**, *73*, 4021–4041.
149. Lorenz, E.N. The predictability of a flow which possesses many scales of motion. *Tellus* **1969**, *21*, 289–307.
150. Zhang, F.; Snyder, C.; Rotunno, R. Effects of moist convection on mesoscale predictability. *J. Atmos. Sci.* **2003**, *60*, 1173–1185.